Citation: Blood Cancer Journal (2012) 2, e64; doi:10.1038/bcj.2012.10

www.nature.com/bcj

ORIGINAL ARTICLE

Rationally engineered nanoparticles target multiple myeloma cells, overcome cell-adhesion-mediated drug resistance, and show enhanced efficacy *in vivo*

T Kiziltepe[1,2,6], JD Ashley[1,6], JF Stefanick[1], YM Qi[1], NJ Alves[1], MW Handlogten[1], MA Suckow[3], RM Navari[4] and B Bilgicer[1,2,5]

In the continuing search for effective cancer treatments, we report the rational engineering of a multifunctional nanoparticle that combines traditional chemotherapy with cell targeting and anti-adhesion functionalities. Very late antigen-4 (VLA-4) mediated adhesion of multiple myeloma (MM) cells to bone marrow stroma confers MM cells with cell-adhesion-mediated drug resistance (CAM-DR). In our design, we used micellar nanoparticles as dynamic self-assembling scaffolds to present VLA-4-antagonist peptides and doxorubicin (Dox) conjugates, simultaneously, to selectively target MM cells and to overcome CAM-DR. Dox was conjugated to the nanoparticles through an acid-sensitive hydrazone bond. VLA-4-antagonist peptides were conjugated via a multifaceted synthetic procedure for generating precisely controlled number of targeting functionalities. The nanoparticles were efficiently internalized by MM cells and induced cytotoxicity. Mechanistic studies revealed that nanoparticles induced DNA double-strand breaks and apoptosis in MM cells. Importantly, multifunctional nanoparticles overcame CAM-DR, and were more efficacious than Dox when MM cells were cultured on fibronectin-coated plates. Finally, in a MM xenograft model, nanoparticles preferentially homed to MM tumors with $\sim$10 fold more drug accumulation and demonstrated dramatic tumor growth inhibition with a reduced overall systemic toxicity. Altogether, we demonstrate the disease driven engineering of a nanoparticle-based drug delivery system, enabling the model of an integrative approach in the treatment of MM.

Blood Cancer Journal (2012) **2,** e64; doi:10.1038/bcj.2012.10; published online 20 April 2012

Keywords: drug delivery; nanoparticle; multiple myeloma; selective targeting; VLA-4; cell-adhesion-mediated drug resistance

INTRODUCTION

Multiple myeloma (MM) is a B-cell malignancy characterized by proliferation of monoclonal plasma cells in the bone marrow (BM). Despite the recent advances in treatment strategies and the emergence of novel therapies, it still remains incurable with a median survival of 3–5 years owing to development of drug resistance.[1,2] A major factor that leads to drug resistance in MM patients is the survival advantages provided by the BM microenvironment. It is well demonstrated that adhesion of MM cells to the BM stroma results in cell-adhesion-mediated drug resistance (CAM-DR), and that the MM cells in the BM microenvironment are much less sensitive to chemotherapeutic agents.[3,4] Anti-adhesion therapy is evolving as a promising approach in oncology, particularly in MM.[5] Therefore, therapeutic agents that have the combined effect of targeting MM cells and inhibiting their adhesion to BM milieu would provide an advantage by overcoming CAM-DR for improved patient outcome.

Very late antigen-4 (VLA-4; also known as $\alpha_4\beta_1$ integrin) is a cell surface heterodimer expressed on cancers of hematopoietic origin, such as lymphomas, leukemias and MM.[4,6–8] In MM, VLA-4 is a key adhesion molecule that acts as a receptor for the extracellular matrix protein fibronectin, and the cellular counter-receptor VCAM-1.[2] Studies demonstrated that VLA-4 has a critical role in CAM-DR of MM cells and provides resistance to first line chemotherapeutics such as doxorubicin (Dox).[4,9] Importantly, inhibition of MM cell adhesion to the BM microenvironment via α_4-integrin blocking antibodies or α_4-siRNA overcomes drug resistance in MM cells.[9–11] Combined, these results suggest VLA-4 as an attractive therapeutic target, both for selective targeting of MM cells, as well as for inhibition of CAM-DR.

Nanotechnology has been recognized by the National Cancer Institute as a paradigm changing opportunity with the potential to make significant breakthroughs in cancer diagnosis and therapy.[12] One of the most important premises of nanotechnology-based drug delivery systems is the enhanced accumulation in tumor tissue due to the leaky vasculature found in the angiogenic vessels seen predominantly in solid tumors.[13,14] Recent evidence in research has established that angiogenesis also has a major role in some hematological malignancies including MM.[15–17] In line with these findings, liposomal Dox has shown beneficial clinical outcome in MM patients in various settings, and has recently been FDA approved in combination with bortezomib in the treatment of relapsed or refractory MM.[18–20] Despite the recent advances in nanoparticle-based therapeutics in MM, the advantages nanomedicine can provide have yet to be harnessed to their full potential in treating MM.

PEGylated micellar nanoparticles have recently gained increased popularity as efficient drug delivery systems as they

[1]Department of Chemical and Biomolecular Engineering, University of Notre Dame, Notre Dame, IN, USA; [2]Advanced Diagnostics and Therapeutics, University of Notre Dame, Notre Dame, IN, USA; [3]Department of Biological Sciences, University of Notre Dame, Notre Dame, IN, USA; [4]Indiana University School of Medicine South Bend, South Bend, IN, USA and [5]Department of Chemistry and Biochemistry, University of Notre Dame, Notre Dame, IN, USA. Correspondence: Dr B Bilgicer, Department of Chemical and Biomolecular Engineering, Department of Chemistry and Biochemistry, University of Notre Dame, 165 Fitzpatrick Hall, Notre Dame, IN 46556-5637, USA.
E-mail: bbilgicer@nd.edu or http://www.nd.edu/~bbgroup
[6]These authors contributed equally to this work.
Received 22 February 2012; accepted 28 February 2012

combine increased stability, high circulation times and a defined size range of 10–100 nm for increased tumor accumulation and decreased systemic toxicity.[21] An important feature of micellar nanoparticles is that they present particularly attractive scaffolds for the multivalent display of multiple functional groups on their surfaces.[22]

Here, we report the rational engineering of a multifunctional nanoparticle that combines traditional chemotherapy with cell targeting and anti-adhesion functionalities for targeted delivery of Dox to MM cells while overcoming CAM-DR. This is accomplished by designing particles that are simultaneously functionalized with controlled numbers of a VLA-4-antagonist peptide and pH-sensitive Dox conjugates. When the nanoparticles are delivered, they target VLA-4 expressing MM cells, inhibit cellular adhesion via VLA-4, and overcome CAM-DR. At the same time, nanoparticle binding to VLA-4 triggers receptor-mediated uptake, which results in active Dox release due to pH-sensitive bond hydrolysis in the acidic endocytic vesicles. Taken together, we demonstrate the disease-driven engineering of a nanoparticle-based drug delivery system, enabling the model of an integrative approach in the treatment of MM.

MATERIALS AND METHODS

Synthesis of peptide- and Dox-conjugated lipids and nanoparticles

Peptides, and peptide/DSPE-PEG2000 lipid conjugates, were synthesized on Wang resin using Fmoc chemistry (peptide synthesis chemicals/reagents from NovaBiochem, Philadelphia, PA, USA; DSPE-PEG2000 from Avanti Lipids, Alabastar, AL, USA). Resin cleavage of all peptide products was done with TFA, purification via RP-HPLC and characterization by MALDI-TOF-MS. Peptide cyclization through disulfide bond formation was performed in 3 ml DMF with 20 μl DIEA by stirring for 8 h at room temperature. For Dox conjugation, DPPE-GA, hydrazine and diisopropylcarbodiimide were mixed in a vial and allowed to react for 4 h at room temperature. Solvent and excess reactants were removed via evaporation under vacuum. Product was re-dissolved in chloroform, mixed with Dox in methanol and coupled over 3 days. Final product was isolated via extraction, and characterized with MALDI-TOF-MS. For nanoparticle formation, nonfunctionalized and functionalized lipids were mixed at desired molar ratios in DCM, followed by solvent removal via evaporation. The mixture was then re-suspended in PBS, and stirred until clear.

Particle size characterization

Dynamic light-scattering analysis was performed via the 90Plus Nanoparticle Analyzer (Brookhaven Instruments, Holtsville, NY, USA) using 658 nm light, at a fixed angle of 90° at 20 °C. Samples were centrifuged for 30 min before analysis to eliminate dust and larger aggregates.

Dox release kinetics

Dox-conjugated nanoparticles ([Dox] = 34.5 μM) were prepared and release rates were analyzed at pH = 7.4, pH = 5.5 and 0.24 N HCl. Amount of free Dox at different time points were quantified using a Toyopearl AF-Amino-650M resin (Tosoh, Tokyo, Japan) packed column on Agilent series 1200 HPLC (Agilent, Santa Clara, CA, USA) at 477 nm. All data were normalized to total Dox released in HCl solution where hydrolysis was 100% within ~5 min.

Cell culture

All cell lines were obtained from ATCC (Manassas, VA, USA), and were cultured as previously described.[23]

Flow cytometry

α_4- and β_1-integrin subunits were detected using anti-CD49d (PE) or anti-CD29 (FITC) antibodies (BD Biosciences, San Jose, CA, USA). Isotype matched antibodies were used as negative controls. Apoptotic cells were detected with Annexin-V (FITC) antibody (BD Pharmingen, San Diego, CA, USA). Cells were analyzed with Guava EasyCyte flow cytometer (Millipore, Billerica, MA, USA).

Cell-binding assay

MM cells were incubated on ice, for 1 h, with FITC-labeled peptides in binding buffer (25 mM Tris, 150 mM NaCl, 1.5 mM $MgCl_2$, 1.5 mM $MnCl_2$, 5 mM glucose, 1.5 mM BSA). Cells were washed twice and analyzed with Guava EasyCyte flow cytometer. FITC-labeled scrambled peptide was used as nonspecific control, and was subtracted from each data point.

Adhesion assay

The Vybrant Cell Adhesion Assay Kit (Molecular Probes, Grand Island, NY, USA) was used according to the manufacter's instructions. Briefly, calcein-labeled MM cells were added to fibronectin-coated 96-well plates (40 μg/ml) in adhesion buffer (RPMI-1640/ 2% FBS) for 2 h. To evaluate the adhesion inhibitory effects of the VLA-4 antagonist peptides, or peptide functionalized nanoparticles, calcein-labeled cells were added to fibronectin-coated plates and immediately treated with the inhibitory agents. Nonadherent cells were removed by washing with PBS. Adherent cells were quantitated in a fluorescence multi-well plate reader.

Cellular uptake studies

Cells were incubated at 37 °C with rhodamine-labeled nanoparticles in complete media for the indicated time points, and were analyzed with flow cytometer. For confocal microscopy experiments, cytospinned cells were fixed with 4% paraformaldehyde and mounted with VectaShield antifade/DAPI (Vector Labs, Burlingame, CA, USA). Cells were visualized by Nikon A1R confocal microscope with a × 40 oil lens (Nikon Instruments, Melville, NY, USA). Image acquisition was performed by Nikon Elements Ar software (Nikon).

Cytotoxicity assays

CCK-8 (Dojindo, Rockville, MD, USA) was used as previously described.[9] To determine cytotoxicity in the presence of fibronectin, MM cells were plated on fibronectin coated plates (40 μg/ml), in adhesion buffer, for 1 h. Cells were then treated with nanoparticles or free Dox in complete media with 10% FBS, for 72 h. BSA coated plates were used as controls.

Western blotting

Western blotting of MM cells was performed as described before.[23]

Immunocytochemistry

Cytospin of drug–treated cells were prepared on slides, and fixed with 4% paraformaldehyde. Slides were stained with γ-H2AX antibody (Cell Signaling, Danvers, MA, USA) and with Alexa Fluor-488-labeled Fab2 (Molecular Probes) as per manufacturer's instructions. Mounted slides (VectaShield antifade/DAPI) were analyzed by Nikon Eclipse TS100 fluorescence microscope at × 60/0.5–1.25 oil, with a Nikon Infinity camera (Nikon).

MM xenograft mouse model

CB.17 SCID mice (Harlan Laboratories, Indianapolis, IN, USA) were irradiated with 150 rad, and inoculated subcutaneously with 5×10^6 NCI-H929 cells. When tumors were palpable, mice were distributed into four groups of 6–8 mice, and were treated intravenously with $NP_{Dox/VLA4-pep}$, NP_{Dox}, free Dox, or vehicle (PBS), on days 1, 3 and 5. Animals were monitored for body weight and tumor volume. In a separate experiment, three tumor challenged mice from each group were killed on day 5 to determine systemic toxicity. Organ weights were measured. For complete blood count analysis, 200 μl of blood was drawn from each mouse via cardiac puncture, immediately mixed with 50 μl of Sequester Solution (Cambridge Diagnostic Products, Fort Lauderdale, FL, USA), and was analyzed with the HemaVet 950 (Drew Scientific, Dallas, TX, USA). Immunohistochemical staining of excised tumors for caspase-3 was performed as formerly described.[24]

Biodistribution studies

Mice were dissected 24 h after injection with 10 mg/kg free Dox or Dox equivalent nanoparticles. Tissues were processed as previously described,[25] and were analyzed for Dox fluorescence (ex. 490 nm/em. 550 nm).

Statistical analysis

Statistical comparisons of continuous variables were carried out by Student's two-tailed *t*-test.

RESULTS

Identification of a VLA-4 antagonist peptide that selectively binds to MM cells and inhibits MM cell adhesion to fibronectin

It is well established that MM cells express VLA-4 receptor, and that VLA-4 facilitates CAM-DR in MM cells.[4,9] We, therefore, validated VLA-4 expression in several MM cell lines, by detecting α_4- and β_1-integrin subunits expression, using flow cytometry (Figure 1a). Several VLA-4-targeting peptides were identified because of the critical role VLA-4 has in cancers.[26–28] None of these peptides, however, have been tested for their specific binding to MM cells, or their adhesion inhibitory effects. Both of these criteria are crucial in our targeting strategy; we therefore generated and screened a small library of peptides from literature. For cellular binding assays, we synthesized FITC-labeled version of the peptides and compared their affinity to MM cells by flow cytometry. We established that the cyclic peptide Tyr-Cys-Asp-Pro-Cys (VLA4-pep; Figure 1b) binds to MM cells with specificity (Figure 1c). Control experiments performed with FITC-labeled nonspecific peptide showed only minimal background binding and was subtracted from each data point. Competitive-binding experiment performed with excess unlabeled VLA4-pep showed inhibition of fluorescence signal indicating that VLA4-pep specifically binds to VLA-4 receptor on MM cells (results not shown). VLA4-pep also proved to be a potent inhibitor of MM cell adhesion to fibronectin in a typical calcein-based cell adhesion assay (Figure 1d). Control experiments done with nonspecific peptide did not show any adhesion inhibitory effects (results not shown). Taken together, VLA4-pep prevailed as the leading VLA-4 antagonist peptide and was incorporated as the targeting and anti-adhesion moiety in the nanoparticles.

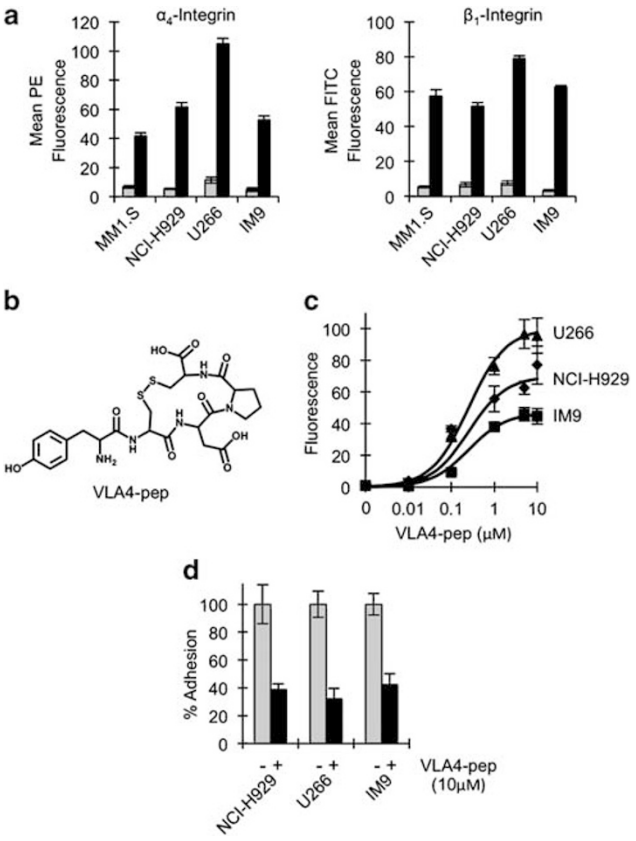

Figure 1. VLA-4 antagonist peptide binds to MM cells, and inhibits their adhesion to fibronectin. (**a**) MM.1S, NCI-H929, U266 and IM9 cell lines all express VLA-4 subunits α_4- and β_1-integrins as determined by flow cytometry. Black columns are primary antibodies and gray columns are isotype controls. (**b**) Structure of VLA-4 antagonist peptide (VLA4-pep). (**c**) Cellular-binding assays were performed using FITC-labeled VLA4-pep and was detected by flow cytometry. Control experiments were done with FITC-labeled nonspecific peptide and the background binding was subtracted for each data point. VLA4-pep binds to U266, NCI-H929 and IM9 cell lines with apparent K_d of $\sim$250 nM. (**d**) VLA4-pep inhibits adhesion of MM cell lines to fibronectin-coated plates. BSA-coated plates were used as controls, and no adhesion of MM cells was observed. No inhibition of adhesion was observed in the control experiments done with nonspecific peptide (results not shown). All experiments were done in triplicates and data represents means ($\pm$s.d.).

Synthesis of VLA-4 targeting, Dox-conjugated multifunctional micellar nanoparticles

The nanoparticles were synthesized from the lipid-PEG block co-polymer, DSPE-PEG2000. This PEG-lipid, when placed in water, is reported to self-assemble and form micelles.[29–31] Their size exploits the enhanced permeation and retention (EPR) effect and prevents their entry through healthy endothelium pores.[32,33] Meanwhile, PEG conjugation increases the micelle's solubility, biocompatibility, provides stealth against the reticuloendothelial system (RES) and improves circulation time.[29] DSPE-PEG2000 lipid has a low critical micellar concentration (CMC) of 5–10 μM, allowing for experimentation at therapeutically relevant concentrations without lipid dissociation.[29,31] DSPE-PEG2000 lipid also has a terminal primary amine version allowing for facile conjugation of various molecular moieties.

For incorporation of VLA4-pep into the nanoparticles, VLA4-pep/DSPE-PEG2000 conjugates were synthesized using a synthetic strategy that was developed in our group using solid support methodology as outlined in Figure 2a. VLA4-pep was first synthesized on a Wang resin using Fmoc protocols, followed by the reaction of succinic anhydride at the N-terminal amine to generate a carboxylic acid group at the terminus. This newly generated carboxylic acid group on the resin bound peptide was activated, and DSPE-PEG2000-NH_2 lipid was introduced in anhydrous DMF to promote amide coupling. The peptide-PEG-lipid conjugate was cleaved from the resin using a TFA cocktail, purified via HPLC and characterized by MALDI-TOF-MS. Dox/DPPE-GA lipid conjugation was accomplished using a pH-sensitive hydrazone chemistry to provide controlled drug release (Figure 2b).[34] Hydrazine was first coupled to the carboxylic head group of the lipid, followed by the conjugation of Dox. The conjugate was purified via extraction into chloroform.

Multifunctional micelles were prepared by mixing DSPE-PEG2000, VLA4-pep/DSPE-PEG2000 conjugate and Dox/DPPE-GA conjugate at desired molar ratios (Figure 2c). Each micelle comprises $\sim$90 lipid molecules,[29,35] and their relative monodispersity allows for incorporation of precise numbers of functionalized lipids per particle to provide control over the valency of the targeting peptide and drug loading. Dynamic light-scattering analysis established that regardless of the number and type of functional moieties included, the particles maintained their original size of $\sim$20 nm (Figure 2d).

Dox was conjugated to the lipids via an acid labile bond to prevent the premature release of the chemotherapeutic and thus

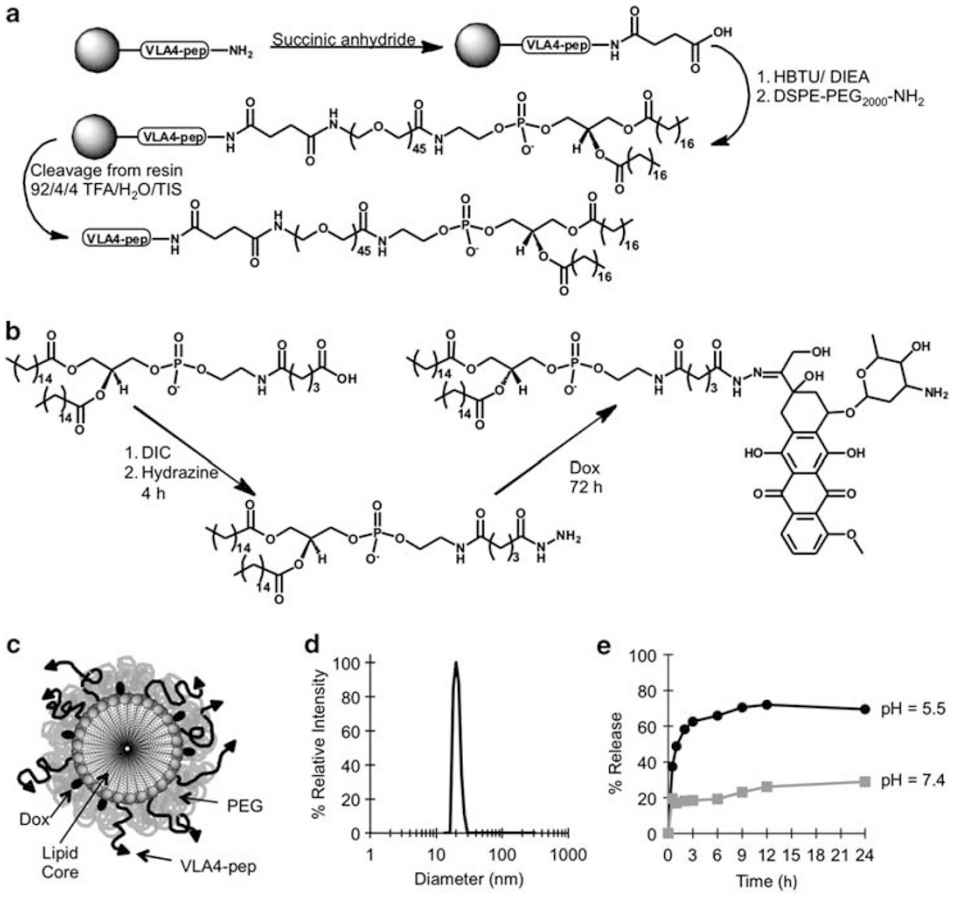

Figure 2. Synthesis and characterization of VLA-4 targeting, Dox-conjugated multifunctional nanoparticles ($NP_{Dox/VLA4-pep}$). (**a**) Schematic illustration of the multifaceted synthetic steps for peptide conjugation to DSPE-PEG2000-NH_2 using solid support. (**b**) Schematic illustration of Dox conjugation to DPPE-GA. (**c**) Illustration of multifunctional micellar nanoparticles that incorporate VLA4-pep and Dox. (**d**) Dynamic light-scattering analysis of nanoparticles. VLA-4 targeting, Dox conjugated ($NP_{Dox/VLA4-pep}$), only Dox conjugated (NP_{Dox}), only VLA4-pep conjugated ($NP_{VLA4-pep}$), Dox and nonspecific peptide conjugated ($NP_{Dox/ns}$), nonspecific-peptide conjugated (NP_{ns}) and bare nanoparticles (NP_{bare}) all gave an average size distribution of $\sim$20 nm. (**e**) Drug release profile of Dox from the nanoparticles in pH = 5.5 and pH = 7.4. Rate of hydrolysis was quantified via HPLC, taking measurements at pre-determined time intervals and observing the absorbance at wavelength of 477 nm. Data shown are from a representative experiment.

nonspecific toxicity. Upon endocytosis of nanoparticles, the acidic environment of endosomes catalyzes the release of active Dox, providing localized delivery inside the tumor cells. The drug release profiles we observed in pH 7.4 and pH 5.5 established that Dox is released from the nanoparticles preferentially under acidic conditions (Figure 2e).

Besides multifunctional nanoparticles with Dox and VLA4-pep conjugates ($NP_{Dox/VLA4-pep}$), other nanoparticles synthesized for control experiments include only Dox conjugated (NP_{Dox}), only VLA4-pep conjugated ($NP_{VLA4-pep}$), Dox and nonspecific peptide conjugated ($NP_{Dox/ns}$), nonspecific-peptide conjugated (NP_{ns}) and bare nanoparticles (NP_{bare}). For imaging and cellular uptake experiments, lissamine rhodamine PE was incorporated in the micelles during formation. In all experiments, the total lipid concentration was above the CMC.

Cellular uptake studies of VLA-4-targeting nanoparticles

Next, we evaluated if VLA4-pep functionalized nanoparticles were taken up by MM cells and determined the optimal peptide valency per micelle for most efficient uptake. Cellular uptake of rhodamine-labeled nanoparticles with varying number of VLA4-pep conjugates ($n = 0-40$/nanoparticle) was studied via flow cytometry. Nanoparticle uptake by NCI-H929 cells increased with increasing VLA4-pep valency up to $n = 20$, then dropped dramatically at $n = 40$ (Figure 3a). Specifically, we observed that 20 peptides per particle yielded the maximum uptake, with up to 10-fold enhancement over that of nontargeted micelles ($n = 0$) after 24 h. We also used NP_{ns} ($n = 20$) as a control, and have observed similar results to that of NP_{bare} (Figure 3b). To establish that uptake of VLA4-pep-conjugated particles were receptor mediated, we performed competition experiments, where MM cells were co-incubated with $NP_{VLA4-pep}$ ($n = 20$) and excess free VLA4-pep. The results showed a dramatic reduction in cellular uptake back to the levels of NP_{bare}, proving receptor involvement in uptake (Figure 3b). It is noteworthy that we observed some nanoparticle uptake even with non-targeted micelles indicating low levels of nonreceptor-mediated uptake (Figures 3a and b).

The studies described above were performed using flow cytometric analysis, as it is a highly accurate quantitative method for studying the effect of peptide valency on uptake. One shortcoming of this method, however, is that it does not discriminate surface bound nanoparticles from internalized ones. Therefore, to show that the nanoparticles are indeed internalized by MM cells, we performed confocal microscopy experiments. These experiments revealed clear uptake of VLA4-pep-conjugated

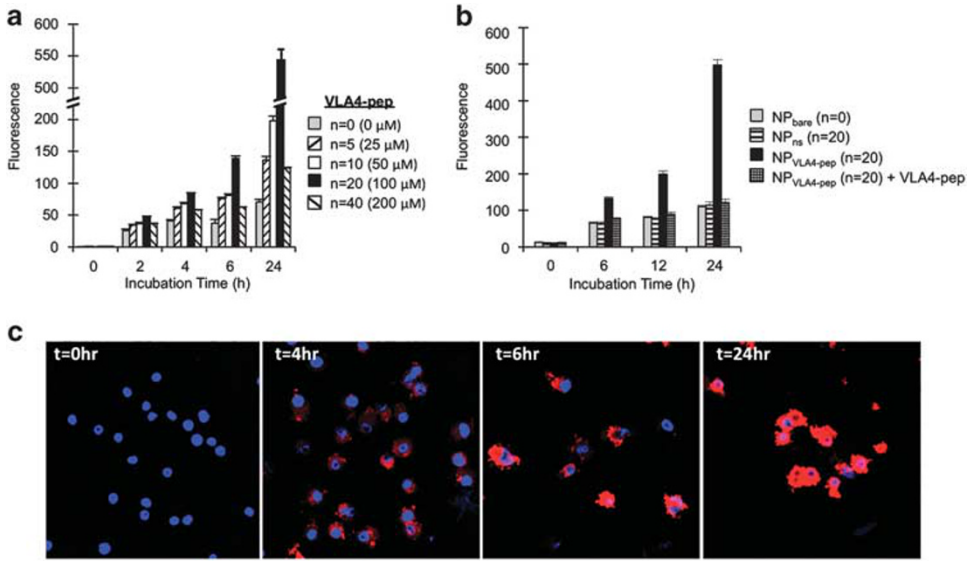

Figure 3. Cellular uptake studies. (**a**) Rhodamine-labeled nanoparticles with varying valency of VLA4-pep conjugates ($n = 0-40$/nanoparticle) were prepared and incubated with NCI-H929 cells at 37 °C for the indicated time points. $N = 20$ peptide conjugates per nanoparticle triggered the most efficient uptake as determined by flow cytometry. (**b**) In a separate experiment, control experiments with NP_{ns}, and competition experiment with excess free VLA4-pep (2 mM) was performed to determine receptor-mediated specificity of nanoparticle uptake. Data represent means (± s.d.) of triplicate experiments. (**c**) Internalization of VLA-4-targeting nanoparticles was confirmed with a Nikon A1R confocal microscope using a ×40 oil lens. Image acquisition was performed by Nikon Elements Ar software.

nanoparticles starting around 4 h and peaking at 24 h (Figure 3c). Altogether, these studies showed efficient receptor-mediated uptake of nanoparticles with optimal uptake properties of $n = 20$ VLA4-pep per micelle. Therefore a valency of 20 peptides per particle was used for rest of our studies.

Multifunctional nanoparticles are cytotoxic against MM cells

We evaluated the cytotoxicity of $NP_{Dox/VLA4-pep}$ against NCI-H929 MM cells using a colorimetric assay. $NP_{Dox/VLA4-pep}$ was significantly cytotoxic to MM cells with IC_{50} values of 0.39 ± 0.06 and 0.13 ± 0.02 μM, at 48 and 72 h, respectively (Figure 4). Control experiments performed with equivalent doses of free Dox showed a moderate advantage over $NP_{Dox/VLA4-pep}$ at 48 h ($IC_{50} = 0.19 \pm 0.04$ μM). This difference was diminished at 72 h, and both free Dox and $NP_{Dox/VLA4-pep}$ showed similar cytotoxic effects ($IC_{50} \sim 0.13$ μM). The difference in cytotoxicity at 48 h is expected given the differences in the cellular uptake mechanisms of free Dox and $NP_{Dox/VLA4-pep}$. While free Dox is taken up via passive diffusion and is active immediately, we designed our nanoparticles to release active Dox only after they are internalized and are exposed to the acidic environment of the endocytic vesicles. Control experiments done with NP_{Dox} showed much reduced cytotoxic effects at 48 and 72 h, further confirming VLA-4's role in nanoparticle uptake (Figure 4). Control experiments performed with $NP_{Dox/ns}$ yielded very similar results to those obtained with non-targeted NP_{Dox} (results not shown). No cytotoxic effects were observed in additional control experiments performed with nanoparticles lacking Dox conjugates, such as NP_{bare} or $NP_{VLA4-pep}$ at equimolar particle concentrations (results not shown).

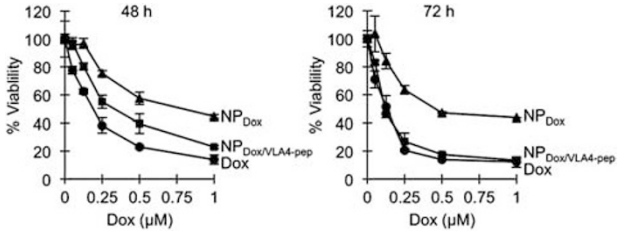

Figure 4. $NP_{Dox/VLA4-pep}$ induces cytotoxicity against MM cells. NCI-H929 MM cells were cultured in the presence of equivalent Dox concentrations of $NP_{Dox/VLA4-pep}$(■), NP_{Dox} (▲), or free Dox (●) for 48 and 72 h. In all cases, cell viability was assessed by cell counting kit-8 (CCK-8), and data represent means (± s.d.) of triplicate cultures. Control experiments performed with $NP_{Dox/ns}$ showed similar results to NP_{Dox}. NP_{bare} and $NP_{VLA4-pep}$ did not show any cytotoxic effects at the concentrations tested (results not shown).

Multifunctional nanoparticles induce DNA double-strand breaks (DSB) and apoptosis in MM cells

It is well established that Dox induces DNA DSB and apoptosis of cancer cells.[36] An early specific cellular response to DSBs in mammalian cells is the phosphorylation of the histone protein H2AX (γ-H2AX), with respective foci formation.[37] Western blot and immunocytochemical analysis showed that both free Dox and $NP_{Dox/VLA4-pep}$ induced H2AX phosphorylation and foci formation in NCI-H929 cells (Figures 5a and b). Furthermore, both agents induced apoptosis as was detected by flow cytometric analysis of the early apoptotic marker Annexin V (Figure 5c), and western blot analysis of PARP and caspase-8 activation (Figure 5d). No significant caspase-9 activation was detected by either agent. Altogether, these results suggest that free Dox and $NP_{Dox/VLA4-pep}$ exert their cytotoxic effects through similar cytotoxic mechanisms. It is noteworthy that no cell death or caspase activation was detected before 36 h at these doses; therefore, DSB formation was not a secondary event of apoptosis.

Multifunctional nanoparticles inhibit adhesion of MM cells to fibronectin and overcome CAM-DR

VLA4-pep serves two major purposes in our nanoparticle design: (i) selective targeting of VLA-4-expressing MM cells and (ii) inhibition of MM cell adhesion to the stroma to overcome

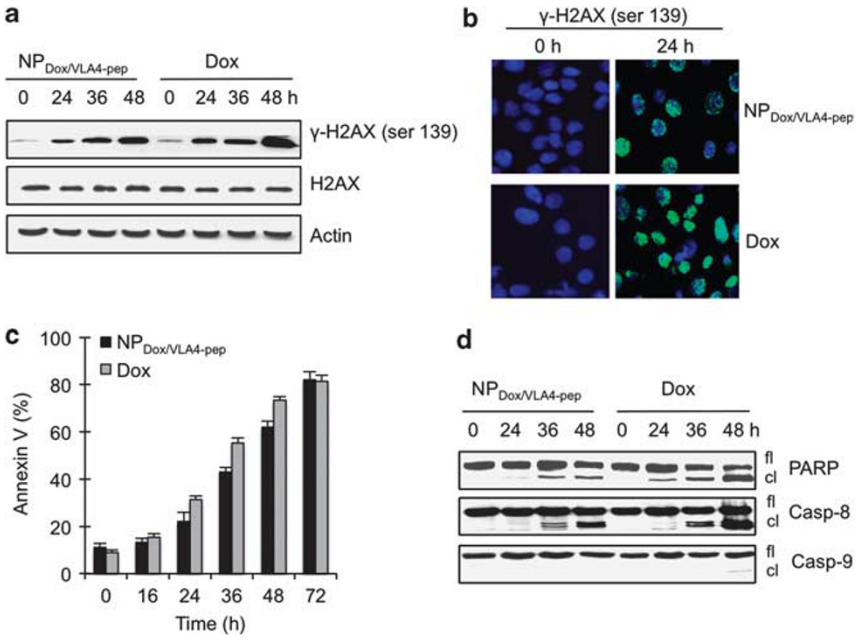

Figure 5. $NP_{Dox/VLA4-pep}$ induces DNA DSBs and apoptosis in MM cells. NCI-H929 cells were treated with 250 nM Dox equivalents of $NP_{Dox/VLA4-pep}$ or free Dox for 0–48 h. (**a**) Phosphorylation of DNA damage response protein H2AX at Ser^{139} was assayed by western blotting. (**b**) Respective H2AX foci formation was assayed by immunocytochemistry (right). Representative images are shown. Apoptosis was assessed by flow cytometry following Annexin V-FITC staining (**c**), and by western blotting for PARP cleavage, and caspase-8 and caspase-9 activation (**d**). For flow cytometric analysis, data represent means (± s.d.) of triplicate experiments. For western blotting, representative images are shown.

CAM-DR. To test if $NP_{Dox/VLA4-pep}$ overcame CAM-DR, first we evaluated its efficiency in inhibiting MM cells adhesion to fibronectin. $NP_{VLA4-pep}$ inhibited adhesion of NCI-H929 cells to fibronectin in a dose-dependent manner (Figure 6a). Dox was not incorporated into the nanoparticles for this assay to eliminate compounding effects that would result from cell death. No inhibition of adhesion was observed with NP_{bare} or NP_{ns} (results not shown). Next, we compared the cytotoxic effects of free Dox or $NP_{Dox/VLA4-pep}$ against MM cells in the presence or absence of fibronectin. Fibronectin-coated plates were used to allow for adhesion of NCI-H929 cells, and BSA-coated plates were used for culturing cells in suspension (MM cells do not adhere to BSA-coated plates). Cells were then incubated with increasing concentrations of $NP_{Dox/VLA4-pep}$ or equivalent concentrations of free Dox. Adhesion of NCI-H929 cells to fibronectin caused CAM-DR in the free Dox treatment group with a three fold IC_{50} shift from 0.13 ± 0.04 to $0.42 \pm 0.09\,\mu M$ (Figure 6b, left). In the $NP_{Dox/VLA4-pep}$ treatment group, however, the IC_{50} values merged towards $\sim 0.2\,\mu M$ both for the adherent and suspension MM cells, indicating that $NP_{Dox/VLA4-pep}$ overcame CAM-DR (Figure 6b, right). The significance of these findings is best illustrated in Figure 6c. When MM cells were cultured in suspension, the efficacy of free Dox in cell killing was similar to that of $NP_{Dox/VLA4-pep}$ with an $IC_{50} \sim 0.13\,\mu M$ (Figure 6c, left). On the other hand, when the cells were cultured in the presence of fibronectin, $NP_{Dox/VLA4-pep}$ ($IC_{50} = 0.15 \pm 0.04\,\mu M$) was more efficacious than free Dox ($IC_{50} = 0.42 \pm 0.09\,\mu M$). These results suggest that $NP_{Dox/VLA4-pep}$ overcame CAM-DR in MM cells.

Multifunctional nanoparticles preferentially home to MM tumors and inhibit tumor growth *in vivo*

To validate the therapeutic efficacy of multifunctional nanoparticles, SCID mice were injected with NCI-H929 tumors, and were sorted into four treatment groups: (i) free Dox, (ii) $NP_{Dox/VLA4-pep}$, (iii) NP_{Dox} and (iv) PBS (control). A pilot study performed to determine the maximum tolerated dose of nanoparticles revealed that 6 mg/kg Dox equivalent $NP_{Dox/VLA4-pep}$, injected intravenously on days 1, 3 and 5, resulted in $\leqslant$15% weight loss during a 2-week period (results not shown). This dose was therefore taken as the maximum tolerated dose for nanoparticles and was used in the *in vivo* study. When the tumors were palpable, each mouse was injected with 6 mg/kg Dox equivalent nanoparticles, or free Dox on days 1, 3 and 5. Both free Dox and $NP_{Dox/VLA4-pep}$ resulted in dramatic tumor growth inhibition (Figure 7a). However, at the dose used, mice in the free Dox group lost a significant amount of body weight by day 7 (>15%), and demonstrated moribundity. Therefore, all animals in the free Dox group were killed on day 7 as a result of significant systemic toxicity (Figure 7b). On the other hand, the $NP_{Dox/VLA4-pep}$ group only lost $\sim$10% body weight during the 2-week study period (Figure 7b). These results indicate that $NP_{Dox/VLA4-pep}$ has a much-improved therapeutic index when compared with free Dox. NP_{Dox} also showed tumor growth inhibition, however, it was significantly less efficacious than $NP_{Dox/VLA4-pep}$ (Figure 7a, right). *Ex-vivo* mechanistic studies performed on tumors dissected on day 5 showed that all drug treatment groups induced apoptosis associated with caspase-3 activation (Figure 7c).

$NP_{Dox/VLA4-pep}$ can expectedly accumulate in the tumor through the VLA-4 targeting functionality as well as the enhanced permeation and retention effect, resulting in reduced systemic toxicity. To evaluate enhanced tumor accumulation, we studied the tissue biodistribution of Dox for all treatment groups. Mice were injected with 10 mg/kg Dox, and tissues were dissected 24 h after drug administration for analysis by fluorescence spectroscopy. No significant difference was detected in the distribution of Dox in lung, kidney, heart, or spleen at 24 h, however, significantly more Dox accumulated in the tumor for the $NP_{Dox/VLA4-pep}$ group when compared with free Dox and NP_{Dox}, reaching to $\sim$10 and $\sim$5 fold higher levels, respectively (Figure 7d). These results are consistent with the enhanced inhibition of tumor growth we observed with $NP_{Dox/VLA4-pep}$ and demonstrate that incorporating VLA4-pep to the nanoparticles enabled enhanced targeting of VLA-4 expressing MM tumors.

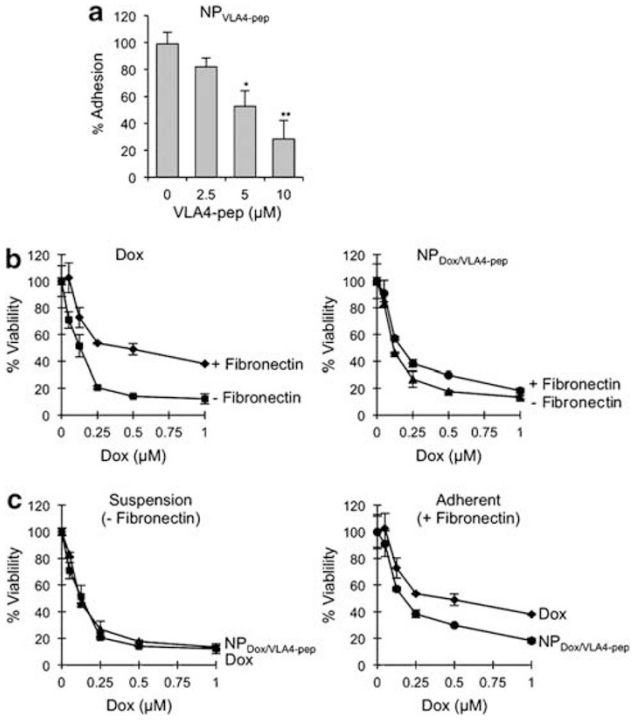

Figure 6. $NP_{Dox/VLA4-pep}$ inhibits adhesion of MM cells to fibronectin and overcomes CAM-DR. (**a**) Calcein-labeled NCI-H929 MM cells were allowed to adhere to fibronectin-coated plates alone, or with increasing concentrations of $NP_{VLA4-pep}$. Nonadherent cells were removed by washing with PBS, and adherent cells were quantitated in a fluorescence multi-well plate reader. Data represents means (± s.d.) of triplicate experiments. $^{*}P<0.05$, $^{**}P<0.01$ when compared with control. (**b**) NCI-H929 cells were allowed to adhere to fibronectin- or BSA-coated plates for 1 h, and then treated with equivalent Dox concentrations of $NP_{Dox/VLA4-pep}$, or free Dox for 72 h. Cell viability was assessed by cell counting kit-8 (CCK-8), and data represent means (± s.d.) of triplicate cultures. (**c**) An alternate illustration of data presented in (**b**).

To evaluate systemic toxicity, complete blood cell count was performed on three additional mice from each group on day 5. Systemic toxicity was detectable in all treatment groups as evident from white blood cell, red blood cell and thrombocyte counts (Figure 7e). The $NP_{Dox/VLA4-pep}$ group, however, showed significantly less toxicity on white blood cell and thrombocytes when compared with free Dox (Figure 7e).

Dox has been associated with clinically significant cardiac and renal toxicity.[38–40] We, therefore, evaluated the effect of the nanoparticles on cardiac and renal weight loss. All drug treatment groups showed only a mild reduction in cardiac mass. There were no detectable difference between $NP_{Dox/VLA4-pep}$ and free Dox (Figure 7f), presumably because of the early time point (day 5) the analysis was performed. On the other hand, we detected a significant difference in kidney weights as $NP_{Dox/VLA4-pep}$ was significantly less toxic than free Dox, and did not cause any significant renal mass loss (Figure 7f). It is noteworthy that, based on biodistribution studies, significant Dox accumulation was evident in kidneys in all treatment groups (Figure 7d). It is possible that the reduced toxicity of the nanoparticles on kidneys is because of the acid-sensitive hydrazone bond, which releases active Dox only after receptor-mediated uptake, or in the acidic microenvironment of the tumor tissue.

Nanoparticles are known to accumulate in and be cleared by the reticuloendothelial system organs (spleen/liver).[14,41] We, therefore, analyzed the effect of nanoparticles on the spleen and liver. All drug treatment groups showed significant accumulation and severe mass loss in spleen, with no detectable difference between nanoparticles and free Dox (Figure 7f). Histopathological examination revealed severe hypoplasia of both erthroid and myeloid elements in all drug treatment groups. Nanoparticles, however, showed only moderate fibrosis, whereas severe fibrosis was evident in the free Dox group (Supplementary Figure 1A). An increased accumulation of nanoparticles in the liver was observed (Figure 7d), however, this was not associated with increased mass loss. To the contrary, $NP_{Dox/VLA4-pep}$ resulted in significantly less weight loss in liver when compared with free Dox (Figure 7f). Increased accumulation in liver without increased toxicity was also shown in previous studies[42,43] and could be due to the acid-sensitive hydrazone bond, which requires an acidic environment to release active Dox. Histopathological analysis revealed moderate hepatocellular hypertrophy and degeneration in free Dox group, whereas only mild effects were observed in the nanoparticle treatment groups (Supplementary Figure 1B). Altogether, these results indicate that $NP_{Dox/VLA4-pep}$ showed decreased overall systemic toxicity than free Dox.

Combined, our results suggest improved therapeutic index for $NP_{Dox/VLA4-pep}$ with dramatic tumor growth inhibition, significantly increased accumulation in tumor, and overall decreased systemic toxicity when compared with free Dox.

DISCUSSION

In this study, we engineered multifunctional micellar nanoparticles that target VLA-4 expressing MM cells selectively, while combining adhesion-inhibitory and cytotoxic effects in a temporal fashion to overcome CAM-DR. In our design, we used peptides as targeting agents, which have several advantages over antibodies such as favorable pharmacokinetics, facile derivatizing and manufacturing, and lower cost.[44] In physiological systems, multiple low-affinity interactions are used to distinguish one cell type from another and to provide selectivity.[45,46] We, therefore, selected a low-affinity VLA-4 antagonistic peptide ($K_d \sim 0.25\,\mu M$; Figure 1c), and used micellar nanoparticles as dynamic self-assembling scaffolds to multivalently present this peptide to target VLA-4 over-expressing MM cells. Receptor-mediated endocytosis is a particularly important aspect in our nanoparticle design, as the acidic environment of the endocytic vesicles is required for active Dox release (Figure 2e). Our results demonstrated that binding of the nanoparticles to VLA-4 triggered receptor-mediated uptake with an optimal valency of 20 peptides per micelle. Although the optimal peptide valency may vary based on the peptide's monovalent affinity, as well as its k_{on} and k_{off} rate constants, these studies validated VLA-4 as a suitable target for targeted drug delivery in MM.

One of the key findings of our study was that when MM cells were allowed to adhere to the extracellular matrix protein fibronectin, $NP_{Dox/VLA4-pep}$ proved to be more efficacious than free Dox, and significantly overcame CAM-DR (Figure 6). These results establish the significance of targeting MM cells as well as their interactions with the microenvironment in the design of more effective novel therapeutics.

Several different mouse models of MM are described.[47] Here, we used a subcutaneous xenograft model of MM for various advantages this model provides, such as the formation of palpable tumors, which makes tumor growth inhibition and biodistribution studies feasible. Our results demonstrated that $NP_{Dox/VLA4-pep}$ preferentially accumulated in the tumor when compared with free Dox and NP_{Dox}. Most importantly, $NP_{Dox/VLA4-pep}$ showed dramatic tumor growth inhibition with decreased overall systemic toxicity, demonstrating improved therapeutic index. It is noteworthy that VLA4-pep targets human VLA-4, and that $NP_{Dox/VLA4-pep}$ may have a different toxicity profile in humans.

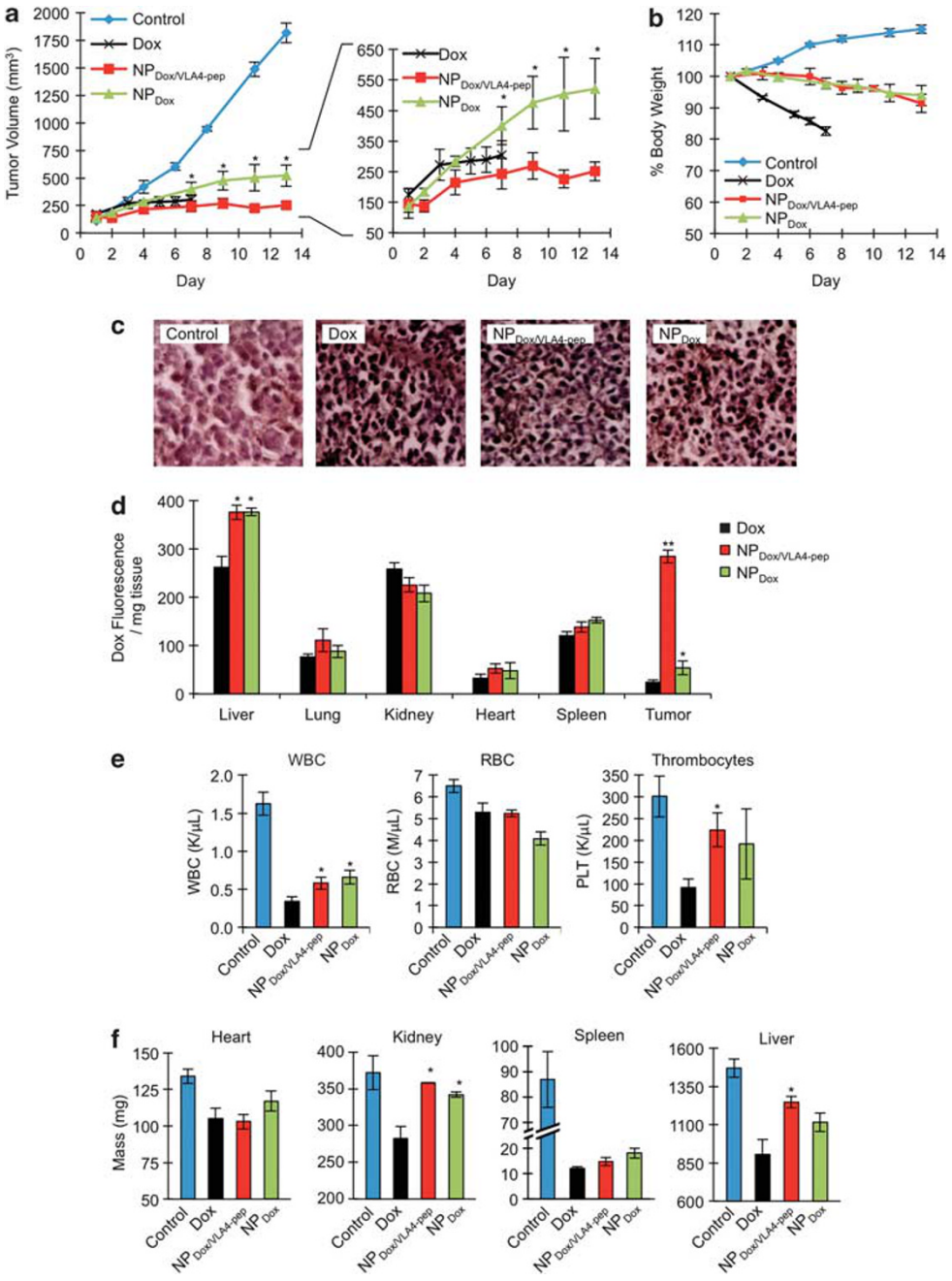

Figure 7. *In vivo* characterization of $NP_{Dox/VLA4-pep}$ in a xenograft model of MM. Tumor bearing SCID mice were injected, intravenously, with free Dox, $NP_{Dox/VLA4-pep}$, or NP_{Dox} at a dose of 6 mg/kg Dox equivalents on days 1, 3 and 5. (**a**) Tumor growth inhibition was detected by caliper measurements. All mice in free Dox group were killed on day 7 because of high systemic toxicity (weight loss $>15\%$). $NP_{Dox/VLA4-pep}$ was significantly more efficacious than NP_{Dox} with $^*P<0.05$. Data shown are means ($\pm$ s.e.) of $n=6-8$ per treatment group. (**b**) Percentage of body weight of the animals as a measure of systemic toxicity. Free Dox group dramatically lost weight ($>15\%$) and demonstrated moribundity by day 7. Therefore, mice in this group were killed on day 7. Only $\sim 10\%$ weight loss was observed with $NP_{Dox/VLA4-pep}$ or NP_{Dox} during the 2-week study period. (**c**) *Ex-vivo* mechanistic analysis of tumors for apoptosis. Three additional mice from each group were dissected on day 5 and tumors were stained for activated caspase-3. Representative images of tumor cross-sections that were captured using a Nikon Eclipse TS100 microscope at $\times 20$ magnification are shown. (**d**) Tissue biodistribution of Dox following treatment. Three mice from each group were treated, intravenously, with 10 mg/kg of Dox equivalent drugs. Mice were killed 24 h after treatment and tissues were analyzed for Dox accumulation. Data shown are means ($\pm$ s.e.). $^*P<0.05$, $^{**}P<0.01$ when compared with free Dox group. (**e**, **f**) Complete blood count and organ weights as a measure of systemic toxicity. Three additional mice from each group were dissected on day 5, and complete blood count (white blood cell, red blood cell and thrombocyte) was performed. (**e**) Weights of excised heart, kidney, spleen and liver are shown. (**f**) Data represent means ($\pm$ s.e.). $^*P<0.05$, when compared with free Dox group.

One shortcoming of the subcutaneous xenograft model is the growth of tumors in the absence of the BM microenvironment. Therefore, the growth and survival advantages provided by the microenvironment, and CAM-DR are not well recapitulated in this model. As a result, the improvement of efficacy observed with $NP_{Dox/VLA4-pep}$ using this model is at best an underestimate.

Studies in our laboratories are underway to evaluate $NP_{Dox/VLA4-pep}$ in a BM model of MM such as the diffuse MM model.[47]

In summary, we have harnessed nanotechnology to develop a combinational therapy approach for MM, where Dox-conjugated nanoparticles selectively targeted VLA-4 expressing MM cells, prevented development of CAM-DR, and dramatically inhibited tumor growth with overall reduced systemic toxicity. Taken together, this study provides the preclinical rationale for the clinical evaluation of VLA-4 targeting, Dox-conjugated multifunctional nanoparticles to improve patient outcome.

CONFLICT OF INTEREST

The authors declare no conflict of interest.

ACKNOWLEDGEMENTS

We thank Notre Dame Integrated Imaging Facility for confocal microscopy, Valerie Schroeder and Freimann Life Science Center for technical support with animal studies, and Center for Environmental Science and Technology for use of DLS. We thank Sarah Chapman for preparing the histology sections. We thank Deborah Donahue and the WM Keck Center for irradiation of mice and CBC analysis. We also thank Dr Gregory Knipp for insightful discussions. This work was supported by Indiana CTSI CTR Grant 371374-31010-20.

REFERENCES

1 Mitsiades CS, Davies FE, Laubach JP, Joshua D, San Miguel J, Anderson KC *et al.* Future directions of next-generation novel therapies, combination approaches, and the development of personalized medicine in myeloma. *J Clin Oncol* 2011; **29**: 1916 – 1923.
2 Hideshima T, Richardson P, Anderson K. Novel therapeutic approaches for multiple myeloma. *Immunol Rev* 2003; **194**: 164 – 176.
3 Sanz-Rodriguez F, Teixido J. VLA-4-dependent myeloma cell adhesion. *Leuk Lymphoma* 2001; **41**: 239 – 245.
4 Damiano J, Cress A, Hazlehurst L, Shtil A, Dalton W. Cell adhesion mediated drug resistance (CAM-DR): role of integrins and resistance to apoptosis in human myeloma cell lines. *Blood* 1999; **93**: 1658 – 1667.
5 Schmidmaier R, Baumann P. ANTI-ADHESION evolves to a promising therapeutic concept in oncology. *Curr Med Chem* 2008; **15**: 978 – 990.
6 Vincent A, Cawley J, Burthem J. Integrin function in chronic lymphocytic leukemia. *Blood* 1996; **87**: 4780 – 4788.
7 Matsunaga T, Takemoto N, Sato T, Takimoto R, Tanaka I, Fujimi A *et al.* Interaction between leukemic-cell VLA-4 and stromal fibronectin is a decisive factor for minimal residual disease of acute myelogenous leukemia. *Nat Med* 2003; **9**: 1158 – 1165.
8 Carpenter RD, Andrei M, Aina OH, Lau EY, Lightstone FC, Liu R *et al.* Selectively targeting T- and B-cell lymphomas: A benzothiazole antagonist of alpha(4)beta(1) integrin. *J Med Chem* 2009; **52**: 14 – 19.
9 Noborio-Hatano K, Kikuchi J, Takatoku M, Shimizu R, Wada T, Ueda M *et al.* Bortezomib overcomes cell adhesion-mediated drug resistance through downregulation of VLA-4 expression in multiple myeloma. *Oncogene* 2009; **28**: 231 – 242.
10 Podar K, Zimmerhackl A, Fulciniti M, Tonon G, Hainz U, Tai YT *et al.* The selective adhesion molecule inhibitor Natalizumab decreases multiple myeloma cell growth in the bone marrow microenvironment: therapeutic implications. *Br J Haematol* 2011; **155**: 438 – 448.
11 Olson D, Burkly L, Leone D, Dolinski B, Lobb R. Anti-alpha 4 integrin monoclonal antibody inhibits multiple myeloma growth in a murine model. *Mol Cancer Ther* 2005; **4**: 91 – 99.
12 US Department of Health and Human Services. National Institute of Health & National Cancer Institute. A strategic initiative to transform clinical oncology and basic research through the directed application of nanotechnology. Available at http://nano.cancer.gov/about_alliance/cancer_nanotechnology_plan, 2004.
13 Maeda H, Wu J, Sawa T, Matsumura Y, Hori K. Tumor vascular permeability and the EPR effect in macromolecular therapeutics: a review. *J Controlled Release* 2000; **65**: 271 – 284.
14 Sapra P, Tyagi P, Allen TM. Ligand-targeted liposomes for cancer treatment. *Curr Drug Deliv* 2005; **2**: 369 – 381.
15 Abe M. Targeting the interplay between myeloma cells and the bone marrow microenvironment in myeloma. *Int J Hematol* 2011; **94**: 334 – 343.
16 Kumar S, Witzig T, Timm M, Haug J, Wellik L, Kimlinger T *et al.* Bone marrow angiogenic ability and expression of angiogenic cytokines in myeloma: evidence favoring loss of marrow angiogenesis inhibitory activity with disease progression. *Blood* 2004; **104**: 1159 – 1165.
17 Singh Bhatti S, Kumar L, Dinda AK, Dawar R. Prognostic value of bone marrow angiogenesis in multiple myeloma: Use of light microscopy as well as computerized image analyzer in the assessment of microvessel density and total vascular area in multiple myeloma and its correlation with various clinical, histological, and laboratory parameters. *Am J Hematol* 2006; **81**: 649 – 656.
18 Hussein M, Anderson K. Role of liposomal anthracyclines in the treatment of multiple myeloma. *Semin Oncol* 2004; **31**: 147 – 160.
19 Chanan-Khan AA, Lee K. Pegylated liposomal doxorubicin and immunomodulatory drug combinations in multiple myeloma: Rationale and clinical experience. *Clin Lymphoma Myeloma* 2007; **7**: S163 – S169.
20 Ning Y, He K, Dagher R, Sridhara R, Farrell AT, Justice R *et al.* Liposomal doxorubicin in combination with bortezomib for relapsed or refractory multiple myeloma. *Oncology* 2007; **21**: 1503 – 1508.
21 Blanco E, Kessinger CW, Sumer BD, Gao J. Multifunctional micellar nanomedicine for cancer therapy. *Exp Biol Med* 2009; **234**: 123 – 131.
22 Sawant RR, Torchilin VP. Multifunctionality of lipid-core micelles for drug delivery and tumour targeting. *Mol Membr Biol* 2010; **27**: 232 – 246.
23 Kiziltepe T, Hideshima T, Ishitsuka K, Ocio EM, Raje N, Catley L *et al.* JS-K, a GST-activated nitric oxide generator, induces DNA double-strand breaks, activates DNA damage response pathways, and induces apoptosis *in vitro* and *in vivo* in human multiple myeloma cells. *Blood* 2007; **110**: 709 – 718.
24 Yang H, Meng Z, Zhang C, Zhang P, Wang Q. Establishing a new rat model of central venous sinus thrombosis and analyzing its pathophysiological and apoptotic changes. *J Neurosci Methods* 2011; **203**: 130 – 135.
25 Laginha K, Verwoert S, Charrois G, Allen T. Determination of doxorubicin levels in whole tumor and tumor nuclei in murine breast cancer tumors. *Clin Cancer Res* 2005; **11**: 6944 – 6949.
26 Lin K, Castro A. Very late antigen 4 (VLA4) antagonists as anti-inflammatory agents. *Curr Opin Chem Biol* 1998; **2**: 453 – 457.
27 Singh J, Adams S, Carter M, Cuervo H, Lee W, Lobb R *et al.* Rational design of potent and selective VLA-4 inhibitors and their utility in the treatment of asthma. *Curr Top Med Chem* 2004; **4**: 1497 – 1507.
28 Jackson D, Quan C, Artis D, Rawson T, Blackburn B, Struble M *et al.* Potent alpha 4 beta 1 peptide antagonists as potential anti-inflammatory agents. *J Med Chem* 1997; **40**: 3359 – 3368.
29 Ashok B, Arleth L, Hjelm R, Rubinstein I, Onyuksel H. *In vitro* characterization of PEGylated phospholipid micelles for improved drug solubilization: Effects of PEG chain length and PC incorporation. *J Pharm Sci* 2004; **93**: 2476 – 2487.
30 Johnsson M, Hansson P, Edwards K. Spherical micelles and other self-assembled structures in dilute aqueous mixtures of poly(ethylene glycol) lipids. *J Phys Chem B* 2001; **105**: 8420 – 8430.
31 Lukyanov A, Gao Z, Mazzola L, Torchilin V. Polyethylene glycol-diacyllipid micelles demonstrate increased acculumation in subcutaneous tumors in mice. *Pharm Res* 2002; **19**: 1424 – 1429.
32 Maeda H, Bharate GY, Daruwalla J. Polymeric drugs for efficient tumor-targeted drug delivery based on EPR-effect. *Eur J Pharm Biopharm* 2009; **71**: 409 – 419.
33 Torchilin VP. Micellar nanocarriers: Pharmaceutical perspectives. *Pharm Res* 2007; **24**: 1 – 16.
34 Bae Y, Alani AWG, Rockich NC, Lai TSZC, Kwon GS. Mixed pH-sensitive polymeric micelles for combination drug delivery. *Pharm Res* 2010; **27**: 2421 – 2432.
35 Kedar U, Phutane P, Shidhaye S, Kadam V. Advances in polymeric micelles for drug delivery and tumor targeting. *Nanomed Nanotechnol Biol Med* 2010; **6**: 714 – 729.
36 Richardson D, Johnson S. Anthracyclines in haematology: preclinical studies, toxicity and delivery systems. *Blood Rev* 1997; **11**: 201 – 223.
37 Burma S, Chen B, Murphy M, Kurimasa A, Chen D. ATM phosphorylates histone H2AX in response to DNA double-strand breaks. *J Biol Chem* 2001; **276**: 42462 – 42467.
38 Ferreira AL, Matsubara LS, Matsubara BB. Anthracycline-induced cardiotoxicity. *Cardiovasc Hematol Agents Med Chem* 2008; **6**: 278 – 281.
39 Giri S, Al-Bayati M, Schelegle E, Mohr F, Margolin S, Du X. Amelioration of doxorubicin-induced cardiac and renal toxicity by pirfenidone in rats. *Cancer Chemother Pharmacol* 2004; **53**: 141 – 150.
40 Burke J, Laucius J, Brodovsky H, Soriano R. Doxorubicin Hydrochloride-associated renal-failure. *Arch Intern Med* 1977; **137**: 385 – 388.
41 Chrastina A, Massey KA, Schnitzer JE. Overcoming *in vivo* barriers to targeted nanodelivery. *Wiley Interdiscip Rev Nanomed Nanobiotechnol* 2011; **3**: 421 – 437.
42 Liu Z, Chen K, Davis C, Sherlock S, Cao Q, Chen X *et al.* Drug delivery with carbon nanotubes for *in vivo* cancer treatment. *Cancer Res* 2008; **68**: 6652 – 6660.
43 Chaudhuri P, Paraskar A, Soni S, Mashelkar RA, Sengupta S. Fullerenol-cytotoxic conjugates for cancer chemotherapy. *ACS Nano* 2009; **3**: 2505 – 2514.
44 Aina O, Sroka T, Chen M, Lam K. Therapeutic cancer targeting peptides. *Biopolymers* 2002; **66**: 184 – 199.

45 Owen RM, Carlson CB, Xu JW, Mowery P, Fasella E, Kiessling LL. Bifunctional ligands that target cells displaying the alpha(v)beta(3) integrin. *Chem BioChem* 2007; **8**: 68 – 82.

46 Mammen M, Choi SK, Whitesides GM. Polyvalent interactions in biological systems: Implications for design and use of multivalent ligands and inhibitors. *Angew Chem Int Edit* 1998; **37**: 2755 – 2794.

47 Mitsiades CS, Anderson KC, Carrasco DR. Mouse models of human myeloma. *Hematol Oncol Clin North Am* 2007; **21**: 1051.

Supplementary Information accompanies the paper on Blood Cancer Journal website (http://www.nature.com/bcj)